Journal of Steroid Biochemistry & Molecular Biology 121 (2010) 98–105

Contents lists available at ScienceDirect

Journal of Steroid Biochemistry and Molecular Biology

journal homepage: www.elsevier.com/locate/jsbmb

A molecular description of ligand binding to the two overlapping binding pockets of the nuclear vitamin D receptor (VDR): Structure-function implications☆

Mathew T. Mizwicki[a,*], Danusa Menegaz[a], Sepideh Yaghmaei[b], Helen L. Henry[a], Anthony W. Norman[a,*]

[a] Department of Biochemistry, University of California, 5470 Boyce Hall, Riverside 92521, CA, USA
[b] Department of Chemistry, University of California, Riverside 92521, USA

ARTICLE INFO

Article history:
Received 11 December 2009
Accepted 6 April 2010

Keywords:
VDR
Non-genomic response
1α,25(OH)$_2$-vitamin D$_3$
Chloride channel
Molecular modeling

ABSTRACT

Molecular modeling results indicate that the VDR contains two overlapping ligand binding pockets (LBP). Differential ligand stability and fractional occupancy of the two LBP has been physiochemically linked to the regulation of VDR-dependent genomic and non-genomic cellular responses. The purpose of this report is to develop an unbiased molecular modeling protocol that serves as a good starting point in simulating the dynamic interaction between 1α,25(OH)$_2$-vitamin D$_3$ (1,25D3) and the VDR LBP. To accomplish this goal, the flexible docking protocol developed allowed for flexibility in the VDR ligand and the VDR atoms that form the surfaces of the VDR LBP. This approach blindly replicated the 1,25D3 conformation and side-chain dynamics observed in the VDR X-ray structure. The results are also consistent with the previously published tenants of the vitamin D sterol (VDS)–VDR conformational ensemble model. Furthermore, we used flexible docking in combination with whole-cell patch-clamp electrophysiology and steroid competition assays to demonstrate that (a) new non-vitamin D VDR ligands show a different pocket selectivity when compared to 1,25D3 that is qualitatively consistent with their ability to stimulate chloride channels and (b) a new route of ligand binding provides a novel hypothesis describing the structural nuances that underlie hypercalceamia.

Published by Elsevier Ltd.

1. Introduction

The vitamin D receptor (VDR) can act as both a nuclear localized classical ligand-dependent transcription factor and membrane receptor. As a transcription factor, the VDR acts as a primary regulator of genes that contain vitamin D response elements (i.e. sequence specific VDR binding sites). As a membrane receptor the VDR acts as a primary regulator of lipid and cytosolic second messengers that modulate the activity of kinases and phosphatases that in-turn can control the opened-state of ion channels [1].

The molecular tools (i.e. vitamin D sterol ligands) used to differentiate non-genomic (extra-nuclear) and genomic (nuclear) signaling differ in their chemistries [2]. Structure-function results obtained with these compounds suggest that the major physicochemical traits of a potent and efficient VDR genomic agonist are: (1) the ability to form hydrogen bonds (H-bonds) with the VDR S237 and R274 residues; (2) the ability to conform to a bowl-shaped molecular geometry (Fig. 1); and (3) a molecular volume that is similar to that calculated for 1α,25(OH)$_2$-vitamin D$_3$ (1,25D3, Fig. 2), the classic hormonal form of vitamin D$_3$. Alternatively the major physicochemical traits of a potent and efficient non-genomic agonist are: (1) the ability to form H-bonds with S237 and R274; (2) the ability to conform to a planar-like molecular geometry (Fig. 1); and (3) a molecular volume that is ≤ to that calculated for 1,25D3 [1].

How the VDR molecule can serve as a receptor molecule for ligands with different shapes and physicochemical traits can be rationalized by the vitamin D sterol (VDS)–VDR conformational ensemble model (Fig. 1). This model posits that the VDR ligand binding domain (LBD) contains two overlapping ligand binding pockets (LBP). The VDR alternative pocket (VDR-AP, Fig. 1) was discovered by superimposing the non-genomic specific agonist 1α,25(OH)$_2$-lumisterol D$_3$ (JN, Fig. 2) on the 1,25D3 pose observed in the VDR X-ray crystal structure such that the side-chain of JN oriented towards the H2/β-sheet surface of the VDR rather than the H3/H12 surface (Fig. 1). As shown in Fig. 1, if the VDR-AP is opened and H12 is closed, the VDR-AP and VDR-GP form a capped channel. According to the VDR ensemble principles this conformation represents one of many VDR local energy minima (i.e. conformational isomers, Fig. 1). From the perspective of the VDR ligand this conformation provides the largest internal sur-

☆ Special issue selected article from the 14th vitamin D workshop held at Brugge, Belgium on October 4–8, 2009.

* Corresponding author. Tel.: +1 951 827 4777.
E-mail addresses: Mathew.mizwicki@ucr.edu (M.T. Mizwicki), Anthony.norman@ucr.edu (A.W. Norman).

0960-0760/$ – see front matter. Published by Elsevier Ltd.
doi:10.1016/j.jsbmb.2010.04.005

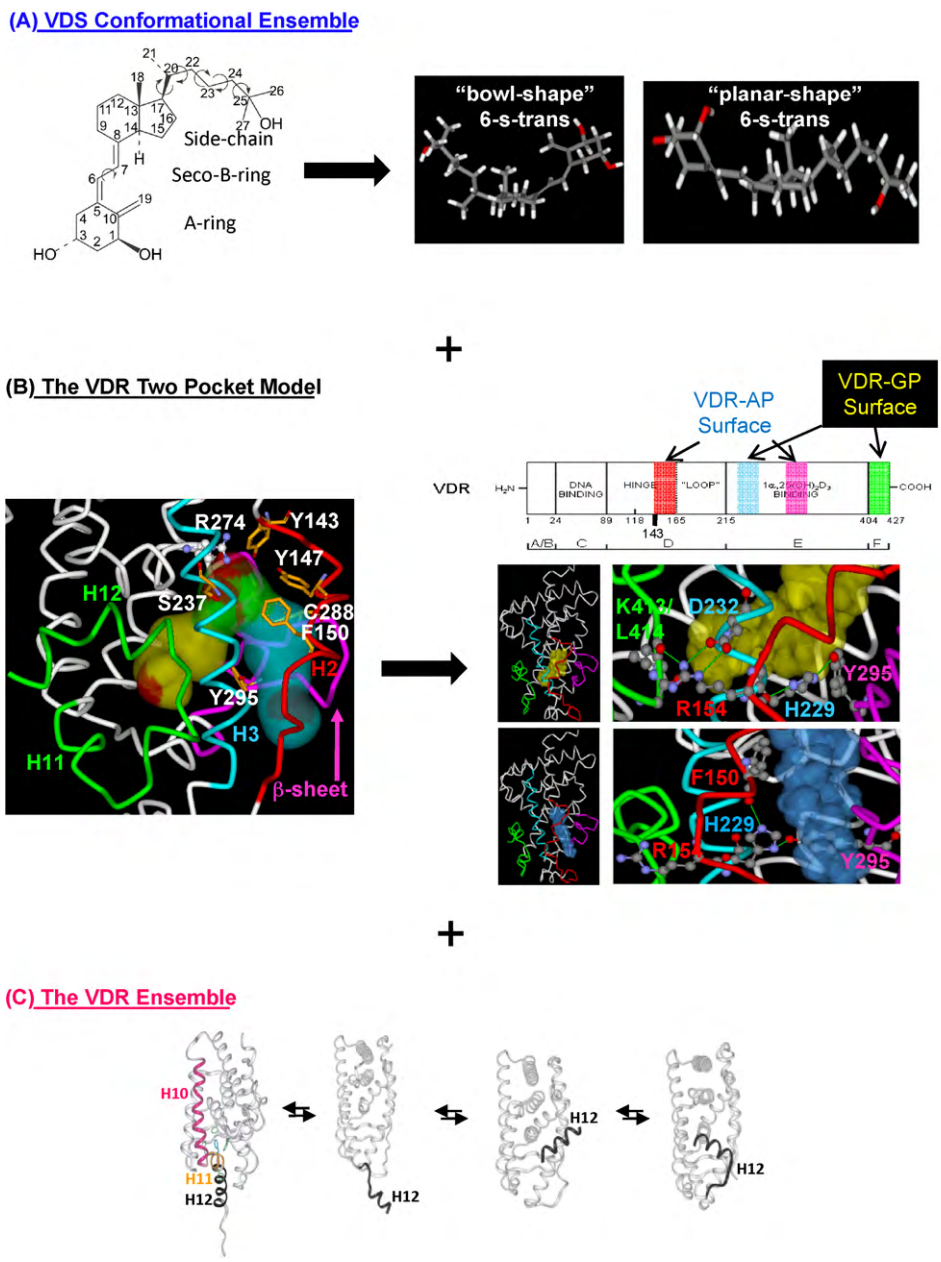

Fig. 1. The vitamin D sterol (VDS)–VDR conformational ensemble model. The VDS–VDR conformational ensemble model can be broken down into three interconnected parts: the VDS conformational ensemble (panel A); the VDR two pocket model (panel B); and the VDR conformational ensemble (panel C). (A) The VDS conformational ensemble is dictated by the number of rotatable bonds in the molecules A-ring, seco-B-ring and side-chain regions. Two of the 6-*s*-*trans* molecular geometries of 1,25D3 that have been shown to form a stable complex with the VDR are depicted in the figure. (B) The VDR two pocket model, posits that an additional steric space in the H2/β-sheet of the VDR molecule opens (blue transparent surface) when the hydrogen bond donor–acceptor relationship between H229 and Y295 switches [3]. The switch is brought about by the rotation of the H229 imidazole R-group. The new pocket formed is termed the VDR alternative binding site (VDR-AP, blue transparent surface). The VDR-AP physically overlaps with the steric space of the VDR genomic pocket (VDR-GP, yellow transparent surface). The VDR-GP is defined by the 1,25D3-VDR X-ray data. The overlapping region of the VDR-GP and VDR-AP is termed the A-ring domain and the residues that form this region are labeled and their wire-frames colored orange. Regions of the VDR that form the molecular surfaces of the VDR-GP and VDR-AP are highlighted in the VDR domain map and their locations indicated in the VDR tertiary structure by color coding the ribbon to the domain map. (C) The implicit VDR conformational ensemble is depicted by using the X-ray coordinates of various apo-holo-NR structures (see the protein data bank). Comparison of the NR structures indicates that helix-12 (H12) is flexible and can sample a number of different conformational states. According to the tenants of the VDS/VDR conformational ensemble model the population distribution of the H12 conformational states is dictated by a given ligands affinity for the VDR-AP and VDR-GP.

face area to sample. Alternatively, when the VDR-AP is closed or VDR-GP occluded by the C-terminal end of H11 (Fig. 1), the surface area of the channel is reduced. Thus different VDR ensembles are posited to be stabilized by different ligands and/or ligand pools (e.g. vitamin D metabolites), because the physicochemical interaction with the dynamic LBP surface will fundamentally differ [1,4–6].

Comparison of the apo-VDR-AP and the apo-VDR-GP structures identified only one major change in the VDR tertiary structure; this was the H-bonding network between the back and front of the VDR LBD [4] (Fig. 1). Breathing of the VDR LBP (i.e. dynamic fluctuation of LBP volume and surface profile) is controlled in-part by a molecular switch that exists between the Y295 (β-sheet)–H229 (H3)–R154 (loop)–K413/L414 (H12) residues, listed back to front

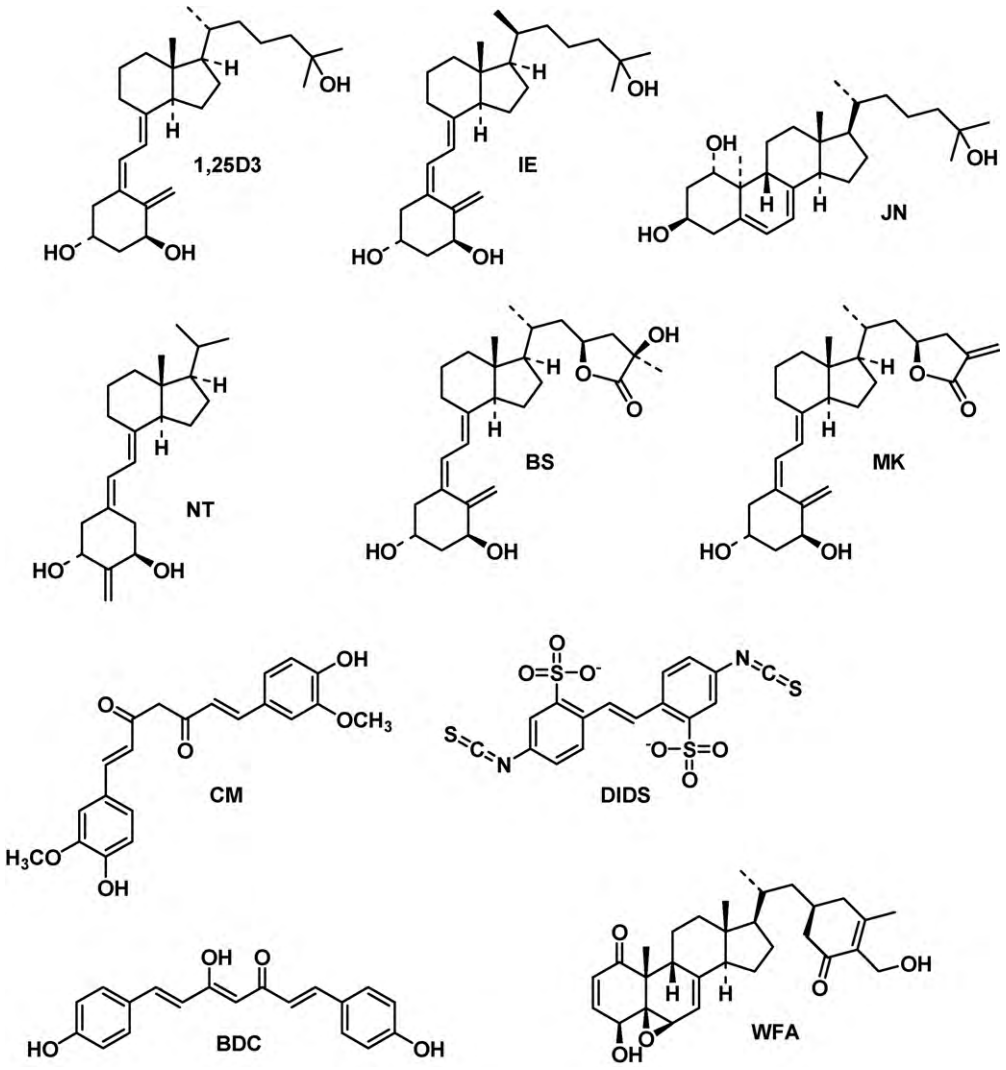

Fig. 2. Chemistry of the VDR ligands. The chemical structures of 1α,25(OH)$_2$-vitamin D$_3$ (1,25D3), 20-epi-1α,25(OH)$_2$-vitamin D$_3$ (IE), 1α,25(OH)$_2$-lumisterol D$_3$ (JN), 2-methylene-19-nor-1α-hydroxyhomopregnacalciferol (NT), 23S,25R-1α,25-(OH)$_2$-D$_3$-26,23-lactone (BS), (23S)-25-dehydro-1α-OH-D$_3$-26,23-lactone (MK), curcumin (CM), 4,4′-Diisothiocyanostilbene-2,2′-disulfonic acid (DIDS), bisdemethoxycurcumin (BDC) and withaferin A (WFA) are shown.

respectively. When the VDR-GP is preferentially occupied by a ligand, these residues form H-bonds that are of paramount importance in holding together the H12 closed conformation (Fig. 1). When 1,25D3 occupies the VDR-AP, the communication between the back (Y295) and front (K413/L414) of the VDR LBD is fractured. The fracture is created by an H-bond donor–acceptor flip-flop between H229 and Y295 (Fig. 1). The H229 residue is therefore central to the communication between the β-sheet and H12 and the gating of the VDR-AP [3,4].

The purpose of this study was to generate a more unbiased and rigorous *in silico* method for simulating the binding of 1,25D3 and other ligands to the VDR. In designing the protocol, three criteria were considered necessary: (1) flexibility in the VDR ligand must be allowed; (2) flexibility in the residues that contact the ligand must be allowed; and (3) superimposition of a VDR ligand on the 1,25D3 X-ray conformer must be avoided. The flexible docking method developed is shown to replicate the 1,25D3 pose and atomic thermal factors observed in the holo-VDR X-ray structure (pdb code: 1db1) [7]. The flexible docking results also support the concept that the VDR-AP exists and is kinetically favored by 1,25D3. Finally, the results also suggest a new mechanism for 1,25D3 binding that provides an explanation for how a genomic superagonist (IE) and a genomic antagonist (MK, Fig. 2) ligand are similar to 1,25D3 in their abilities to function as agonists that activate outwardly rectifying chloride channels.

2. Materials and methods

2.1. Reagents

Withaferin A, Curcumin and Bisdemethoxycurcumin were purchased from ChromaDex, Inc. (Santa Ana, CA 92705) and stocks were made in ethanol. The vitamin D sterols were obtained from the following sources 1,25D3 (Milan Uskokavic, BioXell), MK and BS (Seiichi Ishizuka, Teijin Pharma, Japan) and NT (Abbot Inc., Chicago, IL) and stocks were made in ethanol. DIDS was purchased from Sigma–Aldrich and the stock made in DMSO.

2.2. Molecular modeling

The protocol for generating vitamin D sterol conformational isomers and the flexible docking procedure is described in detail in Mizwicki et al. [8]. The only difference in the protocol used for flexibly docking ligands to the VDR-AP was the fact that 20 VDR R-groups were allowed to be redrawn during the docking process, whereas 15 VDR R-groups were allowed to be redrawn during the

VDR-GP docking process. The number of R-groups allowed to be redrawn for each VDR LBP was determined by trouble shooting what value gave the best cDOCKER scores. The cDOCKER score ranks the complexes saved after a short molecular dynamics simulation is performed. The top 10 scored complexes were then energy optimized and the Gibbs free energy of ligand binding calculated. The top 5 Gibbs free energy of ligand binding values were averaged and the value presented in Table 2. Importantly, this protocol differs from the protocol described in Mizwicki et al. [5] in that solvation effects are considered in the GBMV algorithm used in calculating the $\Delta G_{binding}$ value. The procedure still lacks the assessment of the potential effect entropy changes have on the $\Delta G_{binding}$ value or calculated affinity.

2.3. Ligand binding

The hydroxyapatite protocol used has been published previously [5,8].

2.4. Electrophysiology

TM4 cells (American Type Culture Collection, ATCC, Manasas, VA, USA) were cultured in a 1:1 mixture of Dulbecco's modified Eagle's media (DMEM) and Ham's F12 with the addition of 1 mM L-glutamine, 15 mM HEPES, 1.2 g/l sodium bicarbonate, 100 U/ml penicillin, 100 μg/ml streptomycin, 5% (v/v) horse serum and 2.5% (v/v) fetal calf serum, in a 5% CO_2 humidified atmosphere. For patch-clamp experiments the cells were plated at ~10% density and used within 24–48 h of plating. Cells were washed 3× prior to obtaining a giga seal. Chloride currents were studied in the whole-cell patch-clamp configuration with a Heka EPC-9 amplifier (ALA Scientific Instruments Inc., West bury, NY). Recording pipettes with resistances ranging between 3 and 5 MΩ were fabricated with a DMZ Universal micropipette puller from Drummond capillaries (Drummond Scientific Co., Broomall, PA), coated with Sylgard elastomer (Dow Corning Corp., Midland, MI) to reduce capacitative transients, and fire-polished. Seal resistances ranged from 3 to 15 GΩ. Experiments were carried out at room temperature. Currents were low-pass-filtered at 1 kHz and digitized every 100 μs. Cell membrane capacitance and series resistances were electronically compensated prior to the recording of currents. For the recording of chloride currents, it was used an external solution consisting of (mM): 150 NaCl, 10 $BaCl_2$, 2 $MgCl_2$, 10 glucose, 10 HEPES, pH 7.3. The corresponding pipette solution consisted of (mM): 160 CsCl, 10 $MgCl_2$, 10 HEPES/TEAOH buffer, pH 7.2. Cs^+ and TEA^+ were used to block K^+ channel activity. Currents were activated with 100 ms-pulses between −60 and 80 mV, from a holding potential of −30 mV.

3. Results and discussion

3.1. The vitamin D sterol (VDS) ensemble

Vitamin D_3 (D3) is a seco-steroid and contains an aliphatic cholesterol side-chain; therefore, it differs from most other NR ligands in that it is highly flexible (Fig. 1). To simulate changes in the flexibility or shape of the vitamin D sterol PC_Model GMMX conformational search calculations were performed using the whole molecule (see Section 2). The relative population of 1,25D3 A-ring α/β-chair conformations produced by this method compared well with the equilibrium observed by solution state nuclear magnetic resonance (Table 1) [9]. The 1,25D3 side-chain shows the same population distribution when compared to that obtained in previously published side-chain dot map calculations [5], where the A and seco-B-rings were not present (i.e. only the CD-ring fragment is used, Fig. 1). Lactonization of the 1,25D3 side-chain (e.g. MK and BS, Fig. 2) reduced the disorder of the side-chain, consistent with the reduction in the number of degrees of rotational freedom (Fig. 2) [8].

3.2. The VDR LBP ensemble

Current computational methodologies do not allow for an assessment of global conformational changes in the VDR molecule such as those depicted in the VDR ensemble in Fig. 1. However, R-group (i.e. amino acid side-chain) molecular dynamics or local conformational changes can be simulated. To address how R-group flexibility could alter the dynamics of vitamin D sterol binding, 50 different VDR starting conformations were generated using both the 1,25D3 bound VDR-GP and VDR-AP energy optimized complexes from Mizwicki et al. [5] as the VDR starting structures (see Section 2). In addition, 15 VDR-GP and 20 VDR-AP R-groups respectively were allowed to be redrawn for each of the 5000 theoretical complexes generated by the flexible docking calculation.

3.3. 1,25D3-VDR-GP flexible docking results

The 1,25D3 molecular ensemble (Table 1) was docked to the VDR-GP by generating a 10 $Å^3$ site sphere that encapsulates the VDR-GP ligand binding pocket (LBP, Fig. 3A). After flexible docking, the top 10 scored complexes (Fig. 3B) were energy optimized and the Gibbs free energy of binding ($\Delta G_{binding}$) calculated (see Section 2). The 1,25D3 molecule in the highest affinity 1,25D3-VDR-GP complex superimposes well with the 1,25D3 conformation observed in the X-ray structure (RMSD = 0.85 Å). Therefore the bowl-shaped geometry of 1,25D3 observed in the VDR X-ray study is produced in the generation of the VDS ensemble and selected by the VDR-GP during the flexible docking simulation. The only difference was observed in the position of the terminal side-chain atoms (Fig. 3B). Importantly, the X-ray B-values for these 1,25D3 atoms are significantly higher when compared to the average B-value for all of the 1,25D3 and VDR heavy atoms (i.e. atoms other than hydrogen, see pdb:1DB1). Thus the flexible docking results are consistent with the molecular dynamics observed for 1,25D3 in the X-ray.

The average $\Delta G_{binding}$ value for the 1,25D3-VDR-GP flexible docking complex is in good agreement with the value obtained when the 1,25D3 X-ray pose was used as the only ligand conformation in the flexible docking simulation (Table 2). The flexible docking results indicate that a β-chair A-ring with an equatorial 1α-OH group and a 6-*s-trans* seco-B-ring are selected by the VDR-GP (Table 2), consistent with the X-ray data [7] and structure-function results obtained prior to the solving of the holo-VDR crystal struc-

Table 1
The 1,25D3 conformational ensemble used in flexible docking experiments. 1,25D3 conformational isomers were produced using the GMMX conformational search calculation provided by PC_Model v8.0. Using the search criterion (see Section 2) over 1000 1,25D3 conformations were saved and the top 500 were used in the flexible docking calculation. The breakdown of the A-ring, seco-B-ring and side-chain configurations observed for the top 500 structures are provided in the table. The A-ring α and β-chair population distributions include α and β-twist boats; no boat configurations were observed. The side-chain populations (Pop. A, Pop. B and Pop. C) are defined by the C16–C17–C20–C22 dihedral angles or anti, gauche(+) and gauche(−) geometric isomers (see [4,5] for more details).

VDR ligand	A-ring		Seco-B-ring		Side chain		
	α-chair	β-chair	6-*s-cis*	6-*s-trans*	Pop. A	Pop. B	Pop. C
1,25D3 (500)	52%	48%	26%	74%	68%	14%	18%

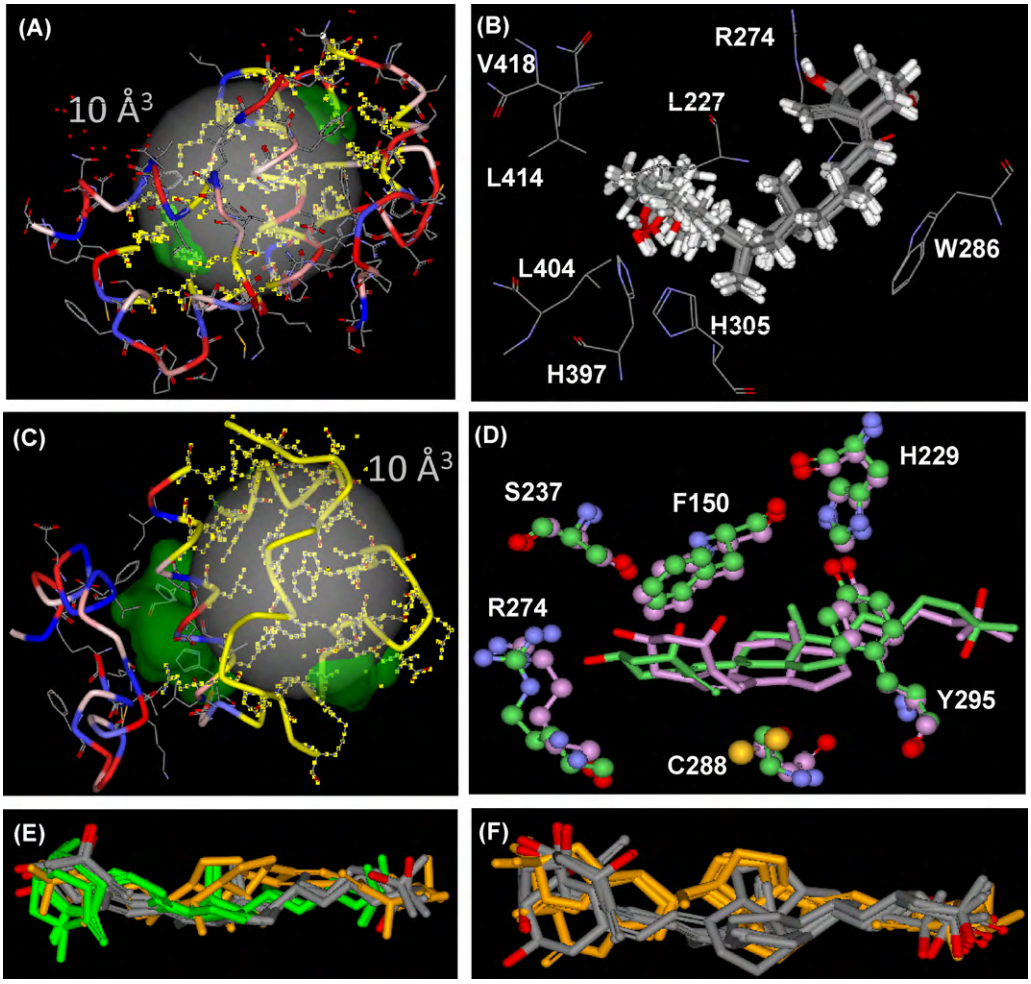

Fig. 3. 1,25D3-VDR-GP and VDR-AP flexible docking results. (A) The VDR-GP 10 Å^3 flexible docking site sphere is shown as a transparent gray sphere. The VDR-GP, ligand binding pocket (LBP) is rendered as a green transparent surface. The VDR R-groups that form the VDR-GP are shown in wire-frame. The VDR backbone is rendered to show its secondary structure that is colored to indicate the relative hydrophobicity of each R-group (red polar to blue non-polar). The R-groups allowed to be redrawn in the flexible docking simulation are highlighted in yellow. (B) The top 10 1,25D3-VDR-GP flexible docking complexes are rendered to show the 1,25D3 molecules as thick gray tube structures and the VDR R-groups thin gray wire-frames. These R-groups are labeled by their one letter code. (C) The VDR-AP 10 Å^3 flexible docking site sphere is shown as a transparent gray sphere. The VDR-AP forms a continuous channel with the VDR-GP. This channel is rendered as a green transparent surface. The VDR R-groups that form the VDR-AP are shown in wire-frame. The R-groups allowed to be redrawn in the flexible docking simulation are highlighted yellow. (D) The alpha chair, 6-*s*-*trans*, pop. A 1,25D3-VDR-AP complexes obtained using the computation methods outlined in Mizwicki et al. [5] (green) and the methods used herein (pink) are heavy atom (i.e. C, N, O, not H) overlaid for comparison. Key amino acids that line the VDR-AP are shown in ball and stick structure. Note the C288 residue forms a number of vdW contacts with the 1,25D3 triene (i.e. seco-B-ring) in both complexes. (E) This presentation shows the top 10 1,25D3-VDR-AP flexible docking complexes. The A-ring first 6-*s*-*trans* poses are colored gray ($n = 5$) (i.e. A-ring occupying the A-ring domain and side-chain oriented towards the H2/β-sheet surface; see Fig. 1B). The A-ring first, 6-*s*-*cis* poses are colored green ($n = 3$). The side-chain first, 1,25D3, 6-*s*-*trans* poses are colored orange ($n = 2$). (F) This panel shows the top 10 BS-VDR-AP flexible docking complexes. The A-ring first, 6-*s*-*trans* poses are colored gray ($n = 6$). The side-chain first, BS, 6-*s*-*trans* poses are colored orange ($n = 4$).

ture [10–12]. Replication of the 1,25D3 X-ray pose and $\Delta G_{binding}$ value was not achieved when the 1,25D3 ensemble was generated using the Discover Studio 2.0 (Accelrys, Inc., San Diego) BEST and CAESER algorithms.

3.4. 1,25D3-VDR-AP flexible docking results

The 1,25D3 conformational ensemble (Table 1) was docked to the VDR-AP by generating a 10 Å^3 site sphere that encapsulates the VDR-AP LBP (Fig. 3C). The highest affinity 1,25D3-VDR-AP complex superimposes well with the best 1,25D3-VDR-AP complex predicted by calculating the potential interaction energy between 1,25D3 and the VDR-AP. Both methods indicated that the preferred conformation of the 1,25D3 molecule accepted by the VDR-AP is the α-chair, 6-*s*-*trans* conformer. The 1,25D3 side-chain shows more disorder, but remains in a low energy, population A orientation (Fig. 3D), giving the molecule an overall planar-like geometry (Fig. 1).

The average1,25D3-VDR-AP $\Delta G_{binding}$ value is calculated to be −40.4 kcal/mole (Table 2); therefore, the 1,25D3-VDR-GP/AP $\Delta G_{binding}$ values are in good agreement with the previously reported, more rudimentary potential interaction energies that suggested 1,25D3 thermodynamically favored the VDR-GP and kinetically favored the VDR-AP. The 1,25D3-VDR-AP flexible docking results also confirm and expand upon the evidence that the VDR-AP can accept more 1,25D3 conformational isomers, including 1,25D3 6-*s*-*cis* rotomers (Fig. 3E). This was not the case for the VDR-GP (Fig. 3B) [1,5,6].

In two of the top 10 scored 1,25D3-VDR-AP complexes, the ligand orientation is reversed within the LBP (Fig. 3E). This places the hydrophobic, highly flexible side-chain atoms in the relatively hydrophilic A-ring domain (Fig. 1); therefore, it is possible that 1,25D3 could access the more hydrophobic VDR-GP through the VDR-AP portal (Fig. 1). This process would be more favored for a ligand with flexibility in its seco-B-ring and side-chain, because it must wiggle around H3 to enter the VDR-GP (Fig. 1). The shape of

Table 2
Flexible docking of VDR ligands to the VDR-GP and VDR-AP. The table summarizes the region of chemical modification with respect to 1,25D3 and the Gibbs free energy of binding ($\Delta G_{binding}$) values (see Section 2) calculated for the given VDR ligand (see Fig. 2 for structures) flexibly docked in the VDR-GP and VDR-AP. The average VDR-GP $\Delta G_{binding}$ value for each VDR ligand is calculated by averaging the values obtained from the top five flexible docking complexes (see Section 2). The average A-ring first VDR-AP $\Delta G_{binding}$ value for each VDR ligand is calculated in the same manner. These average values are well above the theoretical $\Delta G_{binding}$ value that would be derived from the measured equilibrium constants for these sterols (e.g. 1,25D3 K_D = 1.0 nM). The average affinity side-chain first VDR-AP $\Delta G_{binding}$ values are provided for 1,25D3, BS and NT. The frequency of side-chain first complexes observed in the top 10 cDOCKER scored complexes is low for 1,25D3 and NT when compared to NT so the top 5 side-chain first poses in the top 25 VDR-AP complexes were averaged to obtain the reported value. (*) Curcumin (CM) was flexibly docked to the VDR pockets using an ionized and unionized structure. The average CM-VDR-GP $\Delta G_{binding}$ shown in the table is generated from the unionized flexible docking results, if ionized the average VDR-GP $\Delta G_{binding}$ value is positive, reflective of a complex predicted to be unfavored by the Gibbs free energy calculation (e.g. BDC). It is noted that CM and BDC are predicted to bind stably to the VDR-GP by the cDOCKER and LibDock scores, but still prefer the VDR-AP.

VDR ligand	Region of carbon skeleton modified	Average VDR-GP $\Delta G_{binding}$ (kcal/mole)	Average A-ring first VDR-AP $\Delta G_{binding}$ (kcal/mole)	Average side-chain first VDR-AP $\Delta G_{binding}$ (kcal/mole)
1,25D3	Control	−50.7	−40.4	−29.1
25D3	A-ring (C1)	−38.8	−39.9	–
JN	Seco-B-ring	−40.5	−36.2	–
BS	Side-chain	−59.2	−39.9	−37.8
MK	Side-chain	−39.3	−36.5	–
IE	Side-chain (C20)	−44.5	−40.5	–
CM	–	−21.5*	−26.0	–
BDC	–	(+)	−45.7	–
WFA	A-ring/seco-B-ring/side-chain	−30.7	−37.5	–
NT	A-ring/seco-B-ring/side-chain	−42.0	−20.3	−16.8

1,25D3 required to move around H3 is bowl-like (refer to shape of the two pockets together, Fig. 1); therefore, the geometry of the channel may induce the bowl-like shape of 1,25D3 observed in the thermodynamically favored VDR-GP.

The VDR-AP side-chain first VDR-GP binding mechanism differs from the current induced-fit hypothesis that suggests 1,25D3 binds to a somewhat opened H12 conformational state and upon binding induces H12 closure. If a ligand does enter the VDR-GP first, it would require that R274 become exposed by the movement of the C-terminal end of H11 (Fig. 1). Alternatively, the enthalpy barrier is null for VDR-AP opening/closing (i.e. gating) (Fig. 1) and pH-sensitive [3,4]. Another physicochemical feature that is consistent with the hypothesis that ligands first sample the VDR-AP is the observation that the residues forming the surface and internal walls of the VDR-AP are flexible when compared to the VDR-GP (Fig. 1). Thus the intrinsically disordered 1,25D3 ligand is proposed to be better sensed by an intrinsically disordered region of the VDR. Accordingly the VDR-AP could function as a selectivity filter for the VDR-GP and thereby control the fractional occupancy of the VDR-GP and subsequently the transregulation of genes that contain a VDRE [1].

3.5. VDS–VDR-AP vs. VDR-GP ligand A-ring selectivity

We have previously proposed that 25D3 has the same stability in the VDR-AP as 1,25D3 [5]. This was based on the observation that the 3β-OH group of 25D3 and 1,25D3 form H-bonds with S237 and R274 in the VDR-AP and that no H-bonds were formed by the 1α-OH group [1,5,13] (see Fig. 3D). Comparison of the average 1,25D3 and 25D3-VDR-AP flexible docking $\Delta G_{binding}$ values (−40.4 and −39.9 kcal/mole respectively, Table 2) further support this hypothesis. Comparison of the average VDR-GP flexible docking $\Delta G_{binding}$ values for 25D3 and 1,25D3 also substantiate the fact that in order for a ligand to bind to the VDR-GP and therefore be capable of driving gene transcription, it must possess a 1α-OH group and be capable of sampling a bowl-like molecular geometry [6]. Furthermore, the VDR-GP exclusively requires the A-ring be in a β-chair conformation, while in contrast the VDR-AP accepts both A-ring chair forms and their intermediate rotomers (i.e. half-chairs/twist boats, data not shown).

3.6. VDS–VDR-AP vs. VDR-GP ligand seco-B-ring selectivity

This laboratory has previously proposed that 1α,25(OH)$_2$-lumisterol D$_3$ (JN, Fig. 2) can form a complex with the VDR-AP that is of equivalent stability when compared to 1,25D3 [5]. The average JN-VDR-AP $\Delta G_{binding}$ value of −36.2 kcal/mole is consistent with this hypothesis (Table 2). In addition, the JN-VDR-AP and 6-*s*-*cis* 1,25D3-VDR-AP highest affinity complexes superimpose well with one another (data not shown). Unlike, 25D3, JN contains a 1-OH group and therefore, like 1,25D3 is predicted to thermodynamically favor the VDR-GP (Table 2); however, given its fused B-ring JN would be anticipated to have a much slower VDR-GP association rate if access to the VDR-GP was through the VDR-AP side-chain first complex, because this is anticipated to require flexibility in the A/B-ring region of a VDS ligand (Fig. 1).

3.7. VDS–VDR-AP vs. VDR-GP ligand side-chain selectivity

It has been previously proposed that side-chain oxidation of 1,25D3 increases the VDR-AP and VDR-GP stability when compared to 1,25D3 [4]. This hypothesis may explain why downstream metabolites of 1,25D3 can have similar genomic function, but reduced VDR affinity when compared to 1,25D3. The most stable VDR-AP side-chain metabolite complex was formed by BS (Fig. 2) [4]. The protocol used in our previous work was lacking in that solvation and entropic variables were not considered in the computation. The algorithm used in this study to determine the $\Delta G_{binding}$ values considers the effect of solvation.

The average BS-VDR-AP $\Delta G_{binding}$ values indicated that A-ring first BS complex was only as stable as 1,25D3, rather than more stable in the VDR-AP, as originally proposed [4]. It was observed that BS formed a more stable side-chain first complex with the VDR-AP when compared with 1,25D3 −37.8 kcal/mole vs. −29.1 kcal/mole respectively (Table 2 and Fig. 3F). In addition, the reduced flexibility of the BS side-chain (see Fig. 2) could also hinder the ability of BS to wiggle into the VDR-GP when compared to 1,25D3. Thus the original hypothesis that BS has a higher VDR-AP fractional occupancy when compared to 1,25D3 is supported by the pocket dynamics and energetics observed in the flexible docking results.

The 1,25D3 side-chain lactone genomic antagonist [8] (MK, Fig. 2) is somewhat similar in chemistry when compared to 1,25D3 and BS. In the VDR-AP MK formed a complex of similar affinity when compared to 25D3, JN, 1,25D3 and BS (Table 2). Data not presented in the table. Given that the VDR-AP has been physiochemically associated with regulating non-genomic signaling [1,5], MK may be a capable VDR-dependent non-genomic agonist.

3.8. The VDR-AP and superagonist function

The concept that VDR ligands access the VDR-GP through the VDR-AP provides a new mechanistic route to understanding VDR superagonist function. 20-epi-1,25D3 (IE, Fig. 1) is a well studied VDR genomic superagonist. IE differs from 1,25D3 only in the stereochemistry about carbon-20, but this change converts IE into a 10–100-fold more potent genomic agonist when compared to 1,25D3 as determined by the measured EC_{50} of IE and 1,25D3 in inducing expression of reporter genes and differentiation of HL60 cells. Epimerization of C20 also makes 1,25D3 more hypercalcaemic, a therapeutic drawback that remains a mechanistic mystery [14]. Comparison of the 1,25D3 and IE VDR X-ray structures indicates only a minor difference in contacts made with the VDR-GP [15]. Thus no definitive structural evidence correlates with IE superagonism.

According to side-chain dot map calculations IE alters the side-chain conformation distribution to favor more so a northerly orientation with respect to the CD-ring (Fig. 1, Pop. B) [16]. It is this orientation that the VDR two pocket model suggests is required to enter the VDR-GP by wrapping around H3 (see Fig. 1). Therefore it is proposed that IE is a superagonist ligand because (a) it is capable of more quickly occupying the VDR-GP when compared to 1,25D3 and (b) does not undergo C23(S) side-chain oxidation [17], which produces VDS metabolites that have been shown to bind more stably to the VDR-AP when compared to their C24(R) metabolic counterparts [4]. Thus globally IE and its downstream metabolites are proposed to shift the VDS ligand pool to increase the VDR-GP fractional occupancy when compared with 1,25D3 and its pool (i.e. metabolites). In addition, the IE-VDR-AP average $\Delta G_{binding}$ values indicate that IE can form an A-ring first complex with the VDR-AP that has similar affinity to that predicted for 1,25D3 (Table 2).

3.9. Novel VDR ligands favor binding the VDR-AP

Recent evidence demonstrates that curcuminoids (CM and BDC, Fig. 2) bind specifically to the VDR with a low micromolar affinity and form a stable VDR-AP complex [18]. The CM/BDC-VDR-GP and VDR-AP flexible docking results suggest both energetically preferred the VDR-AP (Table 2). This is consistent with CM and BDC possessing a planar molecular shape and identical carbon spacing between the two phenolic–OH groups when compared to the spacing between the C3–OH and the 25-OH group of 1,25D3. Thus CM and BDC contain the physicochemical attributes of a ligand that have been linked to being a good VDR-AP ligand [1].

In searching for other potential VDR ligands present in plant extracts we identified withaferin A (WFA) as a potential VDR ligand. WFA was selected because of its similar structure to JN and BS (Fig. 2) and because it is known to be an anti-inflammatory [19], an attractive function associated with vitamin D3 supplementation. WFA bound specifically to the VDR with a measured affinity of ~2 μM (Fig. 4). The flexible docking results demonstrated that WFA, like CM and BDC energetically preferred the VDR-AP according to the methodology used (Table 2).

3.10. 1,25D3, IE and MK regulation of outwardly rectifying chloride currents in TM4 cells

Given CM, IE and MK form similar complexes with the VDR-AP when compared to 1,25D3, they were screened for their ability to stimulate outward rectifying chloride channels (ORCC) in TM4 Sertoli cells. Like 1,25D3, MK and IE stimulated the opening of ORCC (Fig. 5A). Furthermore, the currents were blocked by co-incubation with equal molar HL, the non-genomic specific antagonist (Fig. 5A). It is observed that IE is a non-agonist when added at 1 nM, but has equal activity when compared to 1,25D3 at 100 nM. This suggests that IE has the same ability to stimulate the non-genomic response, but that it is not as efficient as 1,25D3. This may indicate that the side-chain population A conformational isomer (see Fig. 1 and [13]) is better at accommodating the planar shape requirement suggested to be the optimal geometry for the binding to the VDR-AP A-ring first.

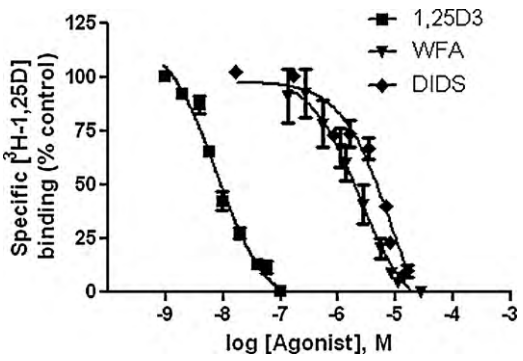

Fig. 4. DIDS and WFA bind specifically to the VDR LBD. Radiolabeled steroid competition was used to generate VDR IC_{50} curves for 1,25D3, WFA and DIDS (see Section 2). The curves represent data pooled from three separate experiments where the concentration of protein was held constant. The IC_{50} values for 1,25D3, WFA and DIDS were measured to be ~8 nM, 2 μM and 8 μM, respectively.

Finally, the stilbene derivative DIDS (Fig. 2) blocked the activation of ORCC by 1,25D3 (Fig. 5B) and was shown to bind specifically to the VDR (Fig. 4). The DIDS VDR IC_{50} (~8 μM) is far lower than the concentrations traditionally used to block ORCC anion currents (50–500 μM).

3.11. The VDR-AP and hypercalcemia

According to the VDS/VDR conformational ensemble model (Fig. 1), vitamin D sterols exert their cellular effects via regulating non-genomic and genomic cellular signaling cascades [1]. Of

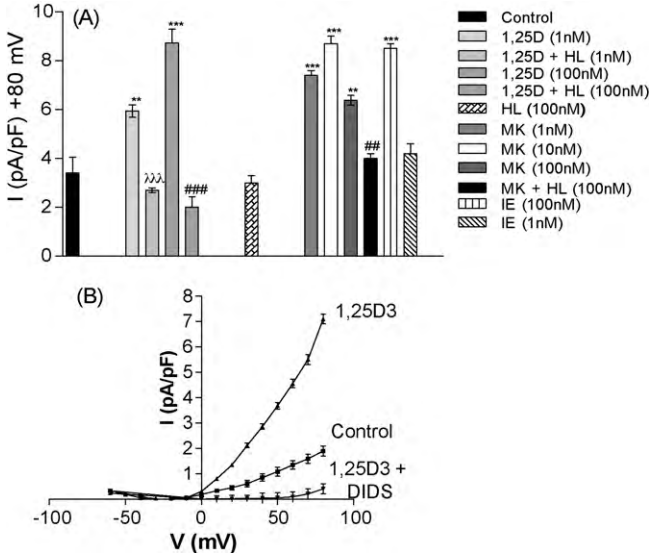

Fig. 5. 1,25D3, MK and IE opening of outwardly rectifying chloride channels (ORCC) channels in TM4 Sertoli cells. (A) Depicts the ORCC measured by whole-cell patch clamp of TM4 cells in the presence or absence of the given concentrations of 1,25D3 and MK (±equal molar HL) or IE. The average mean chloride current measured at +80 mV is depicted in the figure ($n \geq 3$); $^{**}p < 0.01$ compared with control; $^{***}p < 0.001$ compared with control; $^{\#\#}p < 0.001$ compared with VDR ligand group; $^{\#\#\#}p < 0.001$ compared with VDR ligand group. (B) Whole-cell patch-clamp recordings obtained from TM4 cells. The graph plots the applied voltage (mV) against the intensity (I) of the ORCC (pA/pF) observed when 1,25D3 is applied to the bath solution in the presence or absence of DIDS.

the VDR ligands addressed in this study only 1,25D3 and IE trigger hypercalcemia when administered at therapeutic doses. Meanwhile, the VDR ligands MK and BS have both been shown to reduce the calcemic effect of 1,25D3 *in vivo* [20,21]. According to flexible docking and structure-function results, MK differs from 1,25D3 in its VDR-GP stability and ability to stabilize the active conformation of the VDR transcription factor [8]. Alternatively, BS differs from 1,25D3 in its increased fractional occupancy of the VDR-AP (Table 2 and [4]). Thus, increasing the potency of the genomic effects while maintaining the (non-genomic functions of VDR ligands together may underpin the hypercalcemic response.

If hypercalcemia results from a shift in the balance of VDR non-genomic and genomic signaling, then according to the ensemble model increasing the concentration of free 1,25D3 or IE would facilitate an increase in VDR-GP fractional occupancy (the thermodynamically favored 1,25D3/IE-VDR complex). In theory then genomic signaling (e.g. expression of calcium channels and VDR [22,23]) would be enhanced. MK blocks 1,25D3-VDR gene expression [8]; therefore, it could augment the calcemic effect of 1,25D3 by reducing the expression of genes, including but not limited to calcium channels and the VDR itself. Alternatively the BS-VDR-AP models suggest that BS could act to allosterically temper the 1,25D3 calcemic effect by sterically (i.e. physically) blocking 1,25D3 access to the VDR-GP.

Finally, it was recently shown that analog NT (Fig. 2) can suppress PTH and enhance CYP24-OHase without raising serum calcium levels *in vivo* [24]. The later is a trait not observed for 1,25D3 when administered at pharmacologically relevant doses [14]. NT differs from other VDR ligands in this study in that it lacks a side-chain and has a 2-methylene group (Fig. 2). According to the flexible docking results NT differed from 1,25D3, BS, MK and IE in that its ability to form a viable complex with the VDR-AP was reduced. Thus the inability of NT to stimulate an increase in serum calcium and its ability to activate VDR mediated gene transcription may be a functional consequence of its reduced fractional occupancy of the VDR-AP. Furthermore its ability to activate VDR genomic effects in the absence of making van der Waals contacts with H12 of the VDR (Fig. 1) can be attributed to its enhanced fractional occupancy of the VDR-GP when compared to 1,25D3 (Table 2).

4. Conclusions

The unbiased flexible docking protocol and the results generated from its application support the original tenants of the VDS–VDR conformational ensemble model [1,4–6]. The flexible docking technique represents a start point to build upon in future theoretical VDS–VDR ligand binding simulations. The $\Delta G_{binding}$ values presented do not quantitatively correlate to real-life ligand-receptor affinities; however, they qualitatively provide a rationale physicochemical explanation for many VDS–VDR structure-function conundrums. In order to substantiate the claims made, each VDR ligand must be further assayed for both non-genomic and genomic function and additional biochemical characterization of the VDR-GP and VDR-AP complexes obtained. In closing, studying the details of how VDR ligands differ with respect to 1,25D3 in the way they interact with the VDR may provide novel structural/molecular insights into structure-function conundrums within the vitamin D and perhaps other NR-fields.

References

[1] M.T. Mizwicki, A.W. Norman, The vitamin D sterol-vitamin D receptor ensemble model offers unique insights into both genomic and rapid-response signaling, Sci. Signal. 2 (75) (2009) re4.

[2] M.C. Dormanen, J.E. Bishop, M.W. Hammond, W.H. Okamura, I. Nemere, A.W. Norman, Nonnuclear effects of the steroid hormone 1α, 25(OH)$_2$-vitamin D$_3$: analogs are able to functionally differentiate between nuclear and membrane receptors, Biochem. Biophys. Res. Commun. 201 (1994) 394–401.

[3] M.T. Mizwicki, J.E. Bishop, A.W. Norman, Applications of the vitamin D sterol-Vitmain D receptor (VDR) conformational ensemble model, Steroids 70 (2005) 464–471.

[4] M.T. Mizwicki, C.M. Bula, J.E. Bishop, A.W. Norman, New insights into Vitamin D sterol-VDR proteolysis, allostery, structure-function from the perspective of a conformational ensemble model, J. Steroid Biochem. Mol. Biol. 103 (3–5) (2007) 243–262.

[5] M.T. Mizwicki, D. Keidel, C.M. Bula, J.E. Bishop, L.P. Zanello, J.M. Wurtz, D. Moras, A.W. Norman, Identification of an alternative ligand-binding pocket in the nuclear vitamin D receptor and its functional importance in 1α,25(OH)$_2$-vitamin D$_3$ signaling, Proc. Natl. Acad. Sci. U.S.A. 101 (35) (2004) 12876–12881.

[6] A.W. Norman, M.T. Mizwicki, D.P.G. Norman, Steroid hormone rapid actions, membrane receptors and a conformational ensemble model, Nat. Rev. Drug Discov. 3 (2004) 27–41.

[7] N. Rochel, J.M. Wurtz, A. Mitschler, B. Klaholz, D. Moras, The crystal structure of the nuclear receptor for vitamin D bound to its natural ligand, Mol. Cell 5 (1) (2000) 173–179.

[8] M.T. Mizwicki, C.M. Bula, P. Mahinthichaichan, H.L. Henry, S. Ishizuka, A.W. Norman, On the mechanism underlying (23S)-25-dehydro-1{alpha}(OH)-vitamin D3-26,23-lactone antagonism of hVDRwt gene activation and its switch to a superagonist, J. Biol. Chem. 284 (2009) 36292–36301.

[9] R.M. Wing, W.H. Okamura, A. Rego, M.R. Pirio, A.W. Norman, Studies on vitamin D and its analogs VII: Solution conformations of vitamin D$_3$ and 1,25-dihydroxyvitamin D$_3$ by high resolution proton magnetic resonance spectroscopy, J. Am. Chem. Soc. 97 (1975) 4980–4985.

[10] W.H. Okamura, M.N. Mitra, D.A. Procsal, A.W. Norman, Studies on vitamin D and its analogs. VIII. 3-Deoxy-1,25-dihydroxy-vitamin D$_3$, a potent new analog of 1,25-(OH)2-D$_3$, Biochem. Biophys. Res. Commun. 65 (1975) 24–30.

[11] W.H. Okamura, M.N. Mitra, R.M. Wing, A.W. Norman, Chemical synthesis and biological activity of 3-deoxy-1α-hydroxyvitamin D$_3$ an analog of 1α,25-(OH)$_2$-D$_3$, the active form of vitamin D$_3$, Biochem. Biophys. Res. Commun. 60 (1974) 179–185.

[12] D.A. Procsal, W.H. Okamura, A.W. Norman, Studies on the mode of action of calciferol IX: structural requirements for the interaction of 1α,25-(OH)$_2$-vitamin D$_3$ with its chick intestinal receptor system, J. Biol. Chem. 250 (1975) 8382–8388.

[13] M.T. Mizwicki, C.M. Bula, J.E. Bishop, A.W. Norman, A perspective on how the vitamin D sterol/vitamin D receptor (VDR) conformational ensemble model can potentially be used to understand the structure-function results of A-ring modified vitamin D sterols, J. Steroid Biochem. Mol. Biol. (2005) (published on-line October 1).

[14] R. Bouillon, W.H. Okamura, A.W. Norman, Structure-function relationships in the vitamin D endocrine system, Endocr. Rev. 16 (2) (1995) 200–257.

[15] G. Tocchini-Valentini, N. Rochel, J.M. Wurtz, A. Mitschler, D. Moras, Crystal structures of the vitamin D receptor complexed to superagonist 20-epi ligands, Proc. Natl. Acad. Sci. U.S.A. 98 (10) (2001) 5491–5496.

[16] S. Yamada, K. Yamamoto, H. Masuno, M. Ohta, Conformation-function relationship of vitamin D: conformational analysis predicts potential side-chain structure, J. Med. Chem. 41 (9) (1998) 1467–1475.

[17] M.-L. Siu-Caldera, H. Sekimoto, S. Peleg, C. Nguyen, A.-M. Kissmeyer, L. Binderup, A. Weiskopf, P. Vouros, M. Uskokovic, G.S. Reddy, Enhanced biological activity of 1α,25-dihydroxy-20-epi-vitamin D$_3$, the C-20 epimer of 1α,25-dihydroxyvitamin D$_3$, is in part due to its metabolism into stable intermediary metabolites with significant biological activity, J. Steroid Biochem. Mol. Biol. 71 (1999) 111–121.

[18] A. Masoumi, B. Goldenson, S. Ghirmai, H. Avagyan, J. Zaghi, K. Abel, X. Zheng, A. Espinosa-Jeffery, M. Mahanian, P. Liu, M. Hewison, M. Mizwicki, J. Cashman, M. Fiala, 1a, 25-dihydroxyvitamin D3 interacts with curcuminoids to stimulate amyloid-b clearance by macrophages of Alzheimer's disease patients, J. Alzheimers Dis. 17 (2009) 703–717.

[19] R. Maitra, M.A. Porter, S. Huang, B.P. Gilmour, Inhibition of NFkappaB by the natural product Withaferin A in cellular models of Cystic Fibrosis inflammation, J. Inflamm. (Lond.) 6 (2009) 15.

[20] S. Ishizuka, S. Ishimoto, A.W. Norman, Biological activity assessment of 1α, 25-dihydroxyvitamin D$_3$-26, 23-lactone in the rat, J. Steroid Biochem. 20 (1984) 611–615.

[21] S. Ishizuka, D. Miura, K. Ozono, M. Chokki, H. Mimura, A.W. Norman, Antagonistic actions *in vivo* of (23S)-25-dehydro-1α-hydroxyvitamin D$_3$-26,23-lactone on calcium metabolism induced by 1α,25-dihydroxyvitamin D$_3$, Endocrinology 142 (1) (2001) 59–67.

[22] A.J. Karnauskas, J.P. Van Leeuwen, G.J. Van den Bemd, P.P. Kathpalia, H.F. DeLuca, D.A. Bushinsky, M.J. Favus, Mechanism and function of high vitamin D receptor levels in genetic hypercalciuric stone-forming rats, J. Bone Miner. Res. 20 (3) (2005) 447–454.

[23] J.W. Pike, M.B. Meyer, M. Watanuki, S. Kim, L.A. Zella, J.A. Fretz, M. Yamazaki, N.K. Shevde, Perspectives on mechanisms of gene regulation by 1,25-dihydroxyvitamin D3 and its receptor, J. Steroid Biochem. Mol. Biol. 103 (3–5) (2007) 389–395.

[24] L.A. Plum, J.M. Prahl, X. Ma, R.R. Sicinski, S. Gowlugari, M. Clagett-Dame, H.F. DeLuca, Biologically active noncalcemic analogs of 1alpha,25-dihydroxyvitamin D with an abbreviated side chain containing no hydroxyl, Proc. Natl. Acad. Sci. U.S.A. 101 (18) (2004) 6900–6904.